Solid State Communications 257 (2017) 42–46

Contents lists available at ScienceDirect

Solid State Communications

journal homepage: www.elsevier.com/locate/ssc

Communication

Influence of the band bending on the photoconductivity of Li-doped ZnO microwires

J.M. Ferreyra[a,*], G. Bridoux[a,b], M. Villafuerte[a,b], B. Straube[a,b], J. Zamora[a], C.A. Figueroa[a], S.P. Heluani[a]

[a] Laboratorio de Física del Sólido, Facultad de Ciencias Exactas y Tecnología, Universidad Nacional de Tucumán, 4000 Tucumán, Argentina
[b] Consejo Nacional de Investigaciones Científicas y Técnicas - CONICET, Argentina

ARTICLE INFO

Communicated by: F. Peeters

ABSTRACT

Combining photoconductivity and photoluminescence measurements we have studied the band bending behavior with the Li-doping content in ZnO microwires. Our results reveal the presence of in-gap acceptor levels with energies ranging from 100 meV to 600 meV above valence band maximum. We have found that the band bending plays an important role in the photoconductivity modifying the life time of the photocarriers and enhancing the near band edge peak of photoluminescence in Li-doped samples. Using a simple model we have evaluated the influence of the band-bending on the relaxation time for the photoconductivity.

1. Introduction

ZnO is an ideal candidate to build metal-transition oxide optoelectronic devices due to its intriguing surface properties which dominate their physical behavior [1,2]. The surface band bending of ZnO can be tuned by an electric gate [3], the presence of adsorbed oxygen at the surface [4], adsorbed Hydrogen in the $[10\bar{1}0]$ face [5], or polar species like methanol or water [6], leading to the appearance of a two-dimensional electron gas (2DEG) at this surface. At the same time, these surface properties can be critically influenced by the presence of defects, which are mainly segregated at the surface when one of the dimensions is reduced [7]. All these ingredients make ZnO a suitable material to fabricate a new generation of multilayers in which band-bending and defects play a crucial role, evocating the solid work developed in the last decades in GaAs based heterostructures [8]. Native defects, such as zinc interstitials and oxygen vacancies among others [9–11] are responsible for the n-type character of as-grown ZnO since they compensate potential acceptors [12–16]. Such acceptors generate levels in a range between 100 and 160 meV above the valence band maximum (VBM).

A promising candidate to produce stable acceptors in ZnO is Lithium. Its main advantage as acceptor is that it replaces Zn (Li_{Zn}) generating a shallower level than those mentioned above [15,17]. For higher Lithium concentrations, it acts as a shallow donor level due to the fact that it occupies an interstitial site (Li_I), compensating in this way the net hole concentration [18,19]. Several authors point out that the presence of lithium stabilizes the presence of Zn vacancies, making easy the formation of these defects around the impurity [15,20,21]. Some of these independent studies show the presence of Li-related acceptor levels with activation energies ranging from 90 to 900 meV, above VBM [15,22,23]. Obviously, it is the same range of energy usually associated to V_{Zn}. Then, there is a diversity of acceptors levels, deep and shallow, above the VBM.

In this letter, we present further evidence for the shallow nature of a Li acceptor state in ZnO and explore its role in photoconductivity (PC). Literature about ZnO and ZnO:Li is mainly based on photoluminiscence (PL) studies which are useful to analyse electronic levels within the gap, that is, donor or acceptor levels, shallow or deep. PC excitation spectra can also be an important tool to study the transport properties, particularly those affected by levels within the gap [24]. However, despite being a sensitive technique to detect energy levels of defects, it has not been widely used to study defects and impurities. Here we report a systematic study on ZnO:Li microwires (MWs) combining PL and PC and we analyse the behavior of these properties for different Li concentrations. Changes on the PC and PL features with the Lithium concentration are discussed in terms of the band bending (BB) influence which is significant for ZnO. We have developed a simple model for BB that supports our picture. On the other hand, Lithium incorporation in ZnO was corroborated in our previous work [25]. In this study we employ Raman spectroscopy, which turned out to be a suitable technique for this purpose [23,26].

* Corresponding author.
E-mail address: jferreyra@herrera.unt.edu.ar (J.M. Ferreyra).

http://dx.doi.org/10.1016/j.ssc.2017.04.002
Received 23 November 2016; Received in revised form 9 March 2017; Accepted 3 April 2017
Available online 06 April 2017
0038-1098/

2. Experimental

MWs of ZnO were prepared by carbothermal process consistent in the thermal decomposition of the high melting point of ZnO (1975°C) into the low melting point of Zn or Zn suboxides [24,27]. For carbothermal evaporation [28], a pressed ZnO/graphite target (mass ratio of 1:1) was placed on a ceramic holder inside the center of a quartz tube. When the temperature of a programmable tubular furnace reached 1150°C the quartz tube was inserted into it and held there for an hour. Both outlets of the quartz tube were kept open to the ambient air and no carrier gas was applied. The MWs grow directly on the targets, their lengths are close to 1 mm and the diameter vary from 0.1 to 10 μm [24]. For micro-Raman and transport measurements single MWs with diameters of ~10 μm were selected. In order to obtain Li doped ZnO MWs, they were grown in a lithium rich atmosphere. A second ceramic holder containing $LiOH{\cdot}H_2O$ was placed few centimeters beside the first. When the first holder reach 1150 °C the second reach 920 °C (evaporation temperature for $LiOH{\cdot}H_2O$). Corresponding $LiOH{\cdot}H_2O$ mass quantities were used in order to obtain samples with Li nominal contents of 2%, 3%, 5%, and 7%. We label these samples as: ZL2, ZL3, ZL5 and ZL7, respectively, and ZnO for the sample without Li.

High resistivity measurements (above $10^2\,\Omega$cm) were performed using a voltage source-ammeter configuration. An excitation voltage of 4 V was used and the electrical current was measured with a resolution of ~0.5 nA. Measurements were carried out in a standard cryostat equipped with an optical window, a 1000 W Xe lamp plus a monochromator (applied incident light from 200 to 800 nm with an estimated flux density of $\sim 10\,\mathrm{mW cm^{-2}}$). These measurements were made in vacuum ($\sim 10^{-2}$ Torr) at room temperature. Fig. 1 shows a single MW contacted for transport measurements.

The Raman spectrum of the samples was recorded at room temperature in the range 900–50 $\mathrm{cm^{-1}}$ by employing a diode-pump, solid state 532 nm green lasers with 9.0 mW power at the sample for excitation in a Thermoscientific DXR Raman Microscope instrument equipped with CCD detector, a groove density of 900 lines/mm and a spot size of ~2 μm.

3. Results

Fig. 2(b) shows one representative Raman spectrum of a single MW. All typical phonon modes of ZnO are observed, first and second order [23,25,1,29]. The ZnO Raman patterns maintain the main features when the lithium is incorporated: it is worth to note that no additional lines appear and no splitting for any spectra modes.

The non polar E2 (high) mode at 439.2 $\mathrm{cm^{-1}}$ gives information about the strain in the samples [23]. Fig. 2(a) shows the Raman shift of this mode as a function of the lithium content. Each point is an average of the spectra taken on different MWs. Moreover, we repeated each spectrum in order to check repeatability of our micro-Raman set up. Therefore, the standard deviation is marked in the figure by the error bars. Preliminary reports [15,20,26] show that Li, Na, K, P and As impurities incorporate as Zn-substitutional defects in ZnO. The bond lengths are significantly larger than the ideal Zn-O bond length of 0.193 nm, inducing large lattice strains around these impurities. Polarz et al. [23] have observed a low frequency shift of the E2 (high) mode which indicates a compressive stress due to the incorporation of Li_{Zn}. Also, we can see from Fig. 2(a) that the ZL7 sample shows a lower Raman shift than the ZL5 sample. The increasing presence of Li_I at high doping concentrations [20,30] leads to a cancelling effect of the strain provoked by the Li_{Zn} defects.

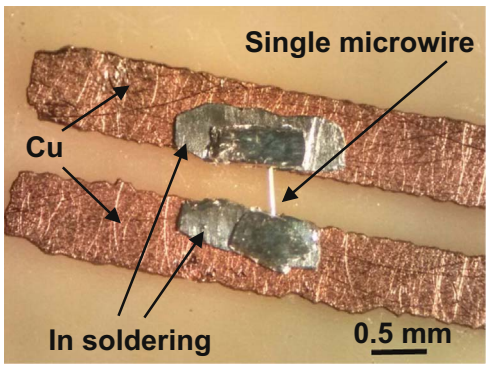

Fig. 1. (Color online) Microwire contacted by cold soldering using In over copper tracks for transport measurements.

The resistivity of the samples after keeping them in darkness for several hours (dark resistivity) was measured. Fig. 2(c) shows that the order of magnitude of the resistivity for ZnO and ZL7 was $10^2\,\Omega$ cm, while for ZL2, ZL3, ZL5 was $10^4\,\Omega$ cm. The increment of resistivity for low lithium contents respect the pure sample is related with the acceptor impurities incorporated (Li_{Zn}) which compensate native donor impurities. The drop of resistivity for high lithium content is due to the increment of Li_I, which increases the donors impurities concentration [18,31].

Fig. 3 shows the photoresistance excitation spectra of single MWs. The photoresistance (PR) is defined as: $PR(\lambda) = [R(\lambda) - R_0]/R_0$, where $R(\lambda)$ and R_0 are the resistances values for each wavelength and for the initial wavelength, respectively. All spectra were taken at a wavelength sweep rate of 0.5 nm/s, from higher to lower wavelengths. The reproducibility of the features of the spectra were checked for different sweep rates larger than 0.5 nm/s and for several MWs for each lithium content. The PR excitation spectra for undoped sample shows a sharp onset at ~371 nm with a maximum slope at 358 nm. Since the photon energy sweeps from lower to higher energies, when the energy of the incident light reaches the gap energy value, a large carrier density will be produced by photo-excitation from VB to CB (see left side of Fig. 4). The wavelength for maximum slope corresponds to 3.4 eV which is very close to ZnO energy gap. Hence, this criteria would be used to measure the energy gap of the samples. In the case of samples ZL2, ZL3 and ZL5, the maximum slope is attained at 371, 366 and 367 nm, respectively, implies an average gap reduction respect to the ZnO case of approximately 95 meV. Then, we have another evidence about the lithium presence as Li_{Zn}, i.e. as shallow acceptor level [15,1,32–34].

The PR spectrum for ZL5 sample (see Fig. 3) shows a clear shoulder at 440 nm. The decrease of PR at the shoulder, indicates excitation of electrons from in-gap levels located 2.8 eV below CB minimum. This characteristic shoulder is also present for samples ZL2 and ZL3, but not for ZL7 sample (see Inset Fig. 3).

Fig. 4 (right panel) shows a sketch of shallow acceptors and in-gap levels and the corresponding transitions to CB for ZnO: Li. The origin of the in-gap levels and more details of this sketch will be discussed below.

Fig. 5 shows the normalized PL spectra at room temperature for ZnO and ZnO: Li. For ZnO sample the peak of Near Band Edge (NBE) is below the limit of detection and the green PL is predominant. When the lithium is incorporated (ZL2, ZL5 and ZL7 samples), a sub-gap peak (around 3.16 eV) and a shoulder at 2.8 eV arise. The first one can be associated to a free electron to neutral acceptor transition (e,A) (transition labeled as 1 in right panel of Fig. 4), giving evidence of shallow acceptor levels located 150–200 meV above the VBM [18,33,35,36] and coincident in energy with the maximum slope of PR excitation spectra for ZnO:Li samples. We identify this acceptor level as Li_{Zn}, as shown in Fig. 4. The shoulder or broad peak at 2.8 eV is attributed to donor-acceptor pair recombination (DAP)(transition labeled as 2 in right panel of Fig. 4), where V_{Zn} are involved [18,19,33] and match with the PR spectra shoulder for ZnO:Li samples. As it was discussed in the Introduction, the incorporation of lithium during the growth of the MWs favours the formation of V_{Zn}, then, shallow (Li_{Zn}) and deep (V_{Zn}) levels of acceptor impurities are produced simulta-

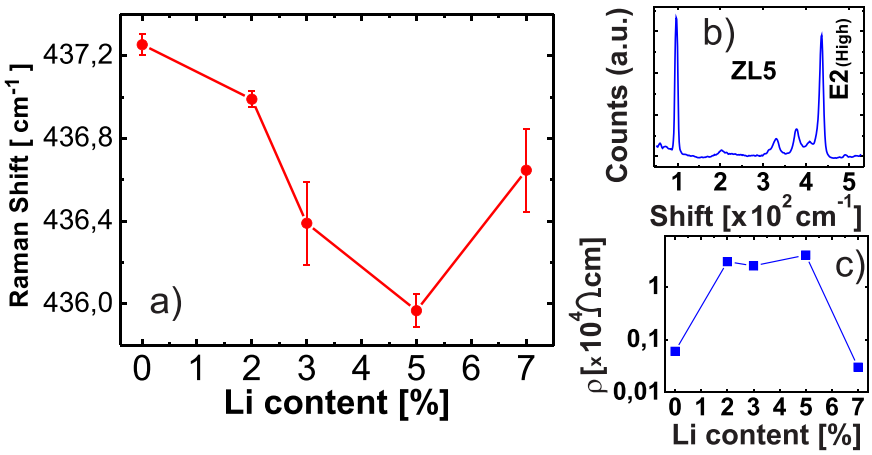

Fig. 2. (Color online) a) Raman shift of the E2 (high) mode for samples with different lithium content. Error bars mark the standard deviation of the measurements. b) Raman spectrum of the sample ZL5. c) Dark resistivity for samples with different lithium content.

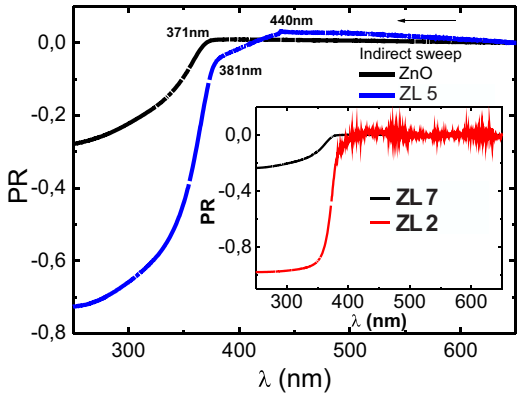

Fig. 3. (Color online) PR excitation spectra for samples ZnO and ZL5. Inset: samples ZL2 and ZL7.

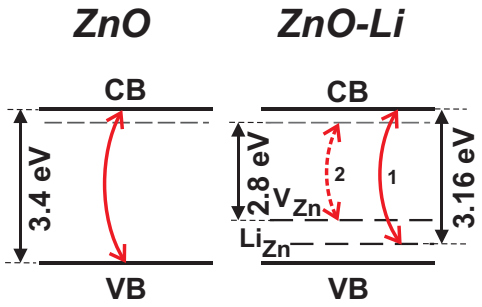

Fig. 4. (Color online) Optical transitions for ZnO and ZnO:Li cases.

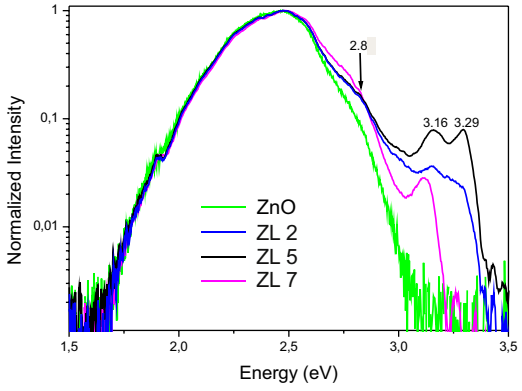

Fig. 5. (Color online) PL vs Energy for samples ZnO and ZnO:Li for different Lithium content.

neously.

It was already reported that in ZnO the conduction band is bended upward near the surface, generating a depletion region of width W (~100 nm) [37,38,4]. On the other side, the depth of light penetration in ZnO is very close to W [24,39]. In ZnO under illumination (UV excitation) the single ionized oxygen vacancies (V_O^*) are dominant and they are responsible of the green band of PL, which is the main contribution in the ZnO spectra (see Fig. 5) [38].

Our results suggest that in samples ZL2 and ZL5, the holes provided by the doping with lithium compensate the negative surface charge and reduce the depletion layer. This fact allows an enhancement of the free electron-free hole recombination increasing the NBE PL (peak at 3.29 eV for ZL5 in Fig. 5) [40]. On the other hand, the presence of acceptor impurities increase the transitions to acceptor levels ((e,A) and DAP), which produce the peak at 3.16 eV and the shoulder at 2.8 eV, which are also present in ZL7. Also, we can see from PL spectra in Fig. 5 that the NBE peak of sample ZL7 is not present. The lithium is incorporated as Li_I, compensating acceptors impurities and arriving to the pure ZnO scenario: the Band Bending (BB) is recovered and the NBE peak disappears [41].

When the light is turned off the PC as a function of time can be fitted by a sum of exponential functions [21,42,40]: $\sum_i e^{t/\tau_i}$, where each term is related to a particular recombination mechanism and τ_i is the characteristic relaxation time for that mechanism. Fig. 6 shows the decaying of PC for four samples: one for ZnO, and three for ZnO:Li with different lithium concentration. There are clear similarities between pure and ZL7 samples on one hand, and between ZL2 and ZL5 on the other hand. For the first pair, the slope evolves slowly with time, for the second one, the slope of PC is steep at the beginning and then change slowly. These differences are confirmed by the different order of magnitude of τ_1 between these two sample pairs (see Table 1, 2nd column) and by the different relaxation times ratios obtained from the fit (see Table 1, 4th column). The order of magnitude of τ_1 for ZL7 is equal to the ZnO sample due to the compensation effect between Li_I and Li_{Zn} (discussed above). Also, these results indicate that for ZL2 and ZL5 samples there are two clearly different recombination mechanisms involved: i)*free electron-free hole* recombination, for short time, and, ii) *free electron-hole released*, for long time [15,21,42,40]. By *free electron (free hole)* we refer to a free carrier into the conduction (valence) band, generated or not by the light. For *hole released* we mean a carrier which previously was trapped by a capture center (Li_{Zn} or V_{Zn}) and subsequently thermally released, clearly this mechanism requires a longer period of time [21]. It is important to elucidate why τ_1 is one order of magnitude lower for samples ZL2 and ZL5. This can be described with similar arguments that was used to explain the effect of the depletion region on PL

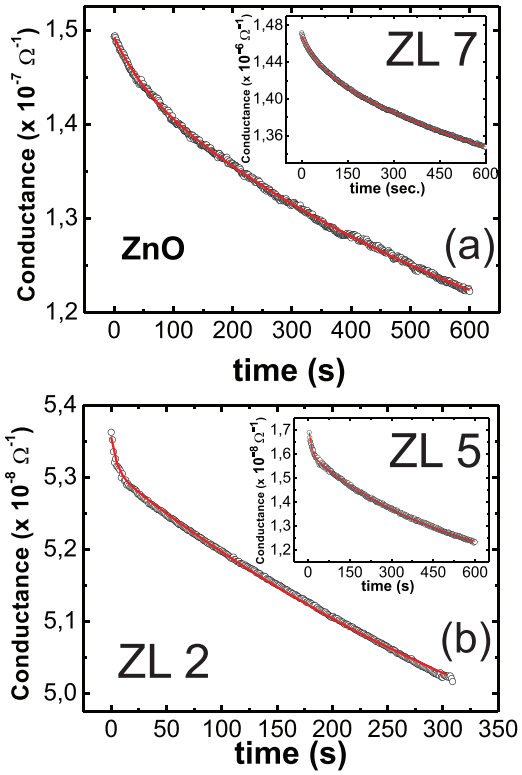

Fig. 6. (Color online) PC relaxation for (a) ZnO (Inset for ZL7)and (b)ZL2 (Inset for ZL5).

Table 1
PC relaxation times (τ_1 and τ_2) obtained from the fitting of the relaxation curves and their ratios for ZnO and ZnO:Li samples.

Sample	τ_1 (s)	τ_2 (s)	τ_2/τ_1
ZnO	52	772	14.8
ZL7	54	722	13.4
ZL5	10	548	54.8
ZL2	5.1	502	98.4

spectra. For the ZnO (top of Fig. 7), the band is bended upward resulting in a strong spatial separation of the electron-hole pair. When this separation is increased, the half-life (τ_1) of these pairs also increases since the overlapping of the electron and hole wave functions is smaller. This behavior is summarized by the expression [43]:

$$<\psi_e|\psi_h>^2 \propto \tau^{-1} \quad (1)$$

Where ψ_e and ψ_h are the electron and hole wave functions, respectively, in a region where the electric potential varies approximately linearly with distance. For the ZnO:Li samples, when the acceptors concentration (N_A) increases and the holes (provided by these impurities) migrate to the surface, they neutralize the native surface charge, reducing the barrier potential of the band bending [4] (see Fig. 7).

In order to understand the effect of the band-bending (BB) over τ_1, we have used a very simple model which approximate the BB with a linear potential. ϕ is related to the width of the layer depletion, W, and the effective donor impurities ($N = N_D - N_A$) by the familiar expression [39,44].

$$W^2 = \frac{2\epsilon_{ZnO}\phi}{N} \quad (2)$$

Where ϵ_{ZnO} is the dielectric constant for ZnO, N_D and N_A are the donor and acceptor impurities concentration. N_D comes from V_O and Zn_I which are typically present in ZnO and N_A comes from Li_{Zn} and

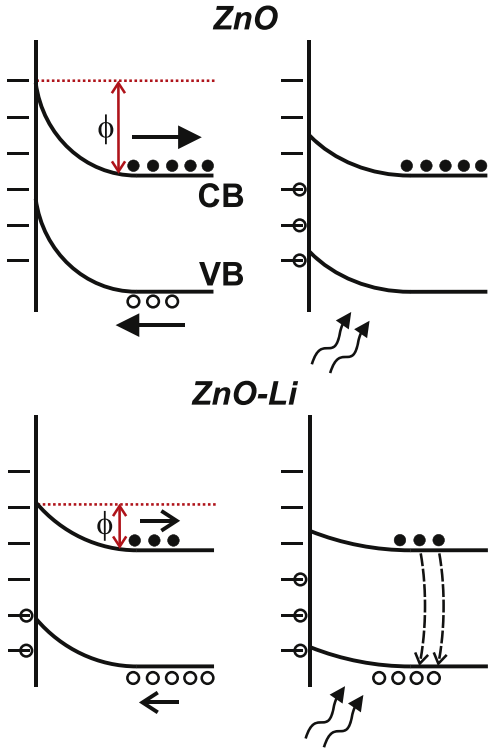

Fig. 7. (Color online) Band bending for ZnO (top) and ZnO:Li (bottom) before the light is on (left) and off (right). When the light is on, the holes generated compensate partially the negative surface charge, so the BB is diminished. For ZnO:Li case, the decrease of BB is bigger because the acceptor impurity and holes concentration is bigger. The band flattening for the ZnO:Li case, reduce considerably the electron-hole separation.

V_{Zn}, as explained above.

For typical values of the parameters involved in the BB equation (Eq. (2)) we would like to determine if it is possible to confine holes, and if that is the case to study the variation of τ (τ_1 in Table 1) with N. Considering that there is a BB confining potential for holes in the z direction (in the Valence Band), $V(z)$, (a barrier for electrons in the conduction band) in the effective mass approximation, it is possible to separate the solution for electrons (holes) in the xy plane, (of the form $exp(i\mathbf{k}_{e(h)}\mathbf{r})$) from the one in the z direction $\chi_{e(h)}(z)$. For the electrons, $\chi_e(z)$ it is one of the two Airy functions: Ai(z) [45], while for holes $\chi_h(z)$ would be a linear combination of the $Ai(z)$ and $Bi(z)$ in the confining region ($0 < z < W$) and a $exp(-bz)$ dependence outside the well ($z > W$) (see Fig. 8 (b) and (d)). From this, and considering the ZnO parameters (effective mass for electron and hole and dielectric constant) it is possible to solve the eigenvalues equation for holes obtaining several localized levels. Since the energy of the ground level is very low compared to the depth of the well (even in the worst case: $N = 10^{16}$ cm^{-3}, $E_1 \sim 0.1\phi$) we can adopt the Fang-Howard wave-function for the ground state [8]: $\chi_h(z) = 2\,\alpha^{3/2} z\, exp(-\alpha z)$. We have numerically evaluated the left side of Eq. (1) for different concentrations (N) in a typical range for ZnO (10^{16} cm^{-3} to 10^{18} cm^{-3}) [39], results are summarized in Fig. 8(e). Taken into account Eq. (1) is clear that τ (τ_1) increase with N, and this happens when the Lithium concentration diminish. Coinciding with this result the Table shows that for samples with low Lithium content, τ_1 decreases respect to the ZnO case.

4. Conclusions

Photoresistance excitation spectroscopy in combination with PL spectroscopy and by investigation of the excitation-relaxation response induced by light allow us to find evidence of significant differences between pure and Li-doped samples, which show in-gap levels presence corresponding to Li_{Zn} and V_{Zn}. These two defects have

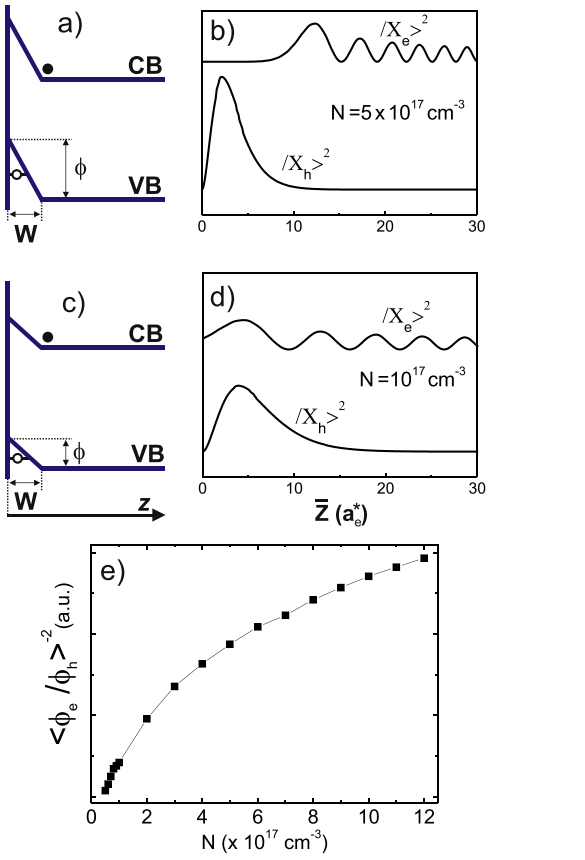

Fig. 8. (Color online) a) and c) show the model for the potential profile in the z direction due to BB for electrons and holes for $N = 5 \times 10^{17}\,\mathrm{cm}^{-3}$ and $N = 1 \times 10^{17}\,\mathrm{cm}^{-3}$ respectively while b) and d) show the corresponding z-dependence wave-functions amplitudes for electrons and holes. e) $\langle\psi_e|\psi_h\rangle^{-2}$ as a function of N.

acceptor behavior, being shallow and deep, respectively. The band bending plays an important role in the PC increasing the life time of the photo-carriers and the behavior of NBE peak in ZnO:Li samples. We developed a simple model in order to find the relationship between the overlapping of the wave functions of the electron and hole, the band bending, the effective concentration of donors near the surface and the PC relaxation time.

Acknowledgements

G.B. and M.V. acknowledge support from CONICET-Argentina. This work was supported by CIUNT under Grant No. 26/E530. We also acknowledge use of the SNMAG facilities.

References

[1] Hadis Morkoc, Umit Ozgur, Zinc Oxide, WILEY-VCH, Weinheim, 2008.
[2] Z. Zang, X. Zeng, J. Du, M. Wang, X. Tang, Opt. Lett. 41 (2016) 3463.
[3] S. Mondal, R.R. Ghimire, A.K. Raychaudhuri, Appl. Phys. Lett. 103 (2013) 231105.
[4] J.C. Moore, C.V. Thompson, Sensors 13 (2013) 9921.
[5] R. Yukawa, K. Ozawa, S. Yamamoto, H. Iwasawa, K. Shimada, E.F. Schwier, K. Yoshimatsu, H. Kumigashira, H. Namatame, M. Taniguchi, I. Matsuda, Phys. Rev. B 94 (2016) 165313.
[6] K. Ozawa, K. Mase, Phys. Rev. B 81 (2010) 205322.
[7] J.C. Fan, K.M. Sreekanth, Z. Xie, S.L. Chang, K.V. Rao, Prog. Mater. Sci. 58 (2013) 874.
[8] J.H. Davies, The Physics of Low-dimensional Semiconductors, Cambridge University Press, New York, 1997.
[9] F. Oba, S.R. Nishitani, S. Isotani, H. Adachi, I. Tanaka, J. Appl. Phys. 90 (2001) 824.
[10] G.W. Tomlins, J.L. Routbort, T.O. Mason, J. Appl. Phys. 87 (2000) 117.
[11] C.G. Van de Walle, Phys. Rev. Lett. 85 (2000) 1012.
[12] G. Xiong, K.B. Ucer, R.T. Williams, J. Lee, D. Bhattacharyya, J. Metson, P. Evans, J. Appl. Phys. 97 (2005) 43528.
[13] D.K. Hwang, H.S. Kim, J.H. Lim, J.Y. Oh, J.H. Yang, S.J. Park, K.K. Kim, D.C. Look, Y.S. Park, Appl. Phys. Lett. 86 (2005) 151917.
[14] Y.R. Ryu, S. Zhu, D.C. Look, J.M. Wrobel, H.M. Jeong, H.W. White, J. Cryst. Growth 216 (2000) 330.
[15] C.H. Park, S.B. Zhang, S.-H. Wei, Phys. Rev. B 66 (2002) 73202.
[16] Eun-Cheol Lee, Y.-S. Kim, Y.-G. Jin, K.J. Chang, Phys. Rev. B 64 (2001) 085120.
[17] E.C. Lee, K.J. Chang, Phys. Rev. B 70 (2004) 115210.
[18] Y.J. Zeng, Z.Z. Ye, J.G. Lu, W.Z. Xu, L.P. Zhu, B.H. Zhao, Appl. Phys. Lett. 89 (2006) 42106.
[19] Y.J. Zeng, Z.Z. Ye, W.Z. Xu, J.G. Lu, H.P. He, L.P. Zhu, B.H. Zhao, Appl. Phys. Lett. 88 (2006) 262103.
[20] J.B. Yi, C.C. Lim, G.Z. Xing, H.M. Fan, L.H. Van, S.L. Huang, K.S. Yang, X.L. Huang, X.B. Qin, B.Y. Wang, T. Wu, L. Wang, H.T. Zhang, X.Y. Gao, T. Liu, A.T.S. Wee, Y.P. Feng, J. Ding, Phys. Rev. Lett. 104 (2010) 137201.
[21] R.H. Bube, Photoconductivity of Solids, John Wiley and Sons, Inc., New York, 1960.
[22] M.G. Wardle, J.P. Goss, P.R. Briddon, Phys. Rev. B 71 (2005) 155205.
[23] S. Polarz, A. Orlov, A. Hoffmann, M.R. Wagner, C. Rauch, R. Kirste, W. Gehlhoff, Y. Aksu, M. Driess, M.W.E. van den Berg, M. Lehmann, Chem. Mater. 21 (2009) 3889.
[24] M. Villafuerte, J.M. Ferreyra, C. Zapata, J. Barzola-Quiquia, F. Iikawa, P. Esquinazi, S.P. Heluani, M.M. de Lima Jr., A. Cantarero, J. Appl. Phys. 115 (2014) 133101.
[25] I. Lorite, B. Straube, H. Ohldag, P. Kumar, M. Villafuerte, P. Esquinazi, C.E. Rodriguez Torres, S. Perez de Heluani, V.N. Antonov, L.V. Bekenov, A. Ernst, M. Hoffmann, S.K. Nayak, W.A. Adeagbo, G. Fischer, W. Hergert, Appl. Phys. Lett. 106 (2015) 082406.
[26] N. Tena Zaera, El oxido de zinc: crecimiento cristalino mediante transporte en fase gaseosa y caracterizacion de propiedades fisicas. Tesis Doctoral. Universitat de Valencia (Servei de Publicacions) 2004.
[27] C. Czekalla, T. Nobis, A. Rahm, B. Cao, J. Zuniga-Perez, C. Sturm, R. Schmidt-Grund, M. Lorenz, M. Grundmann, Phys. Status Solidi B247 (2010) 1282.
[28] L. Chernyak, W. Burdett, M. Klimov, A. Osinsky, Appl. Phys. Lett. 82 (2003) 3680.
[29] J.M. Calleja, M. Cardona, Phys. Rev. B 16 (1977) 3753.
[30] S.U. Awan, S.K. Hasanain, M.S. Awan, S.A. Shah, RSC Adv. 5 (2015) 39828.
[31] S. Chawla, K. Jayanthi, R.K. Kotnala, Phys. Rev. B 79 (2009) 125204.
[32] B.K. Meyer, J. Sann, A. Zeuner, Superlattices Microstruct. 38 (2005) 344.
[33] C. Rauch, W. Gehlhoff, M.R. Wagner, E. Malguth, G. Callsen, R. Kirste, B. Salameh, A. Hoffmann, S. Polarz, Y. Aksu, M. Driess, J. Appl. Phys. 107 (2010) 24311.
[34] Z. Zhang, K.E. Knutsen, T. Merz, A. Yu Kuznetsov, B.G. Svensson, L.J. Brillson, J. Phys. D: Appl. Phys. 45 (2012) 375301.
[35] T. Nakagawa, I. Sakaguchi, K. Matsunaga, T. Yamamoto, H. Haneda, Y. Ikuhara, Nucl. Instrum. Methods Phys. Res. B 232 (2005) 343.
[36] H. Zeng, G. Duan, Y. Li, S. Yang, X. Xu, W. Cai, Adv. Funct. Mater. 20 (2010) 561.
[37] Z. Zhang, J.T. Yates Jr., Chem. Rev. 112 (2012) 5520.
[38] K. Vanheusden, C.H. Seager, W.L. Warren, D.R. Tallant, J.A. Voigt, Appl. Phys. Lett. 68 (1996) 403.
[39] L.L. Yang, Q.X. Zhao, M.Q. Israr, J.R. Sadaf, M. Willander, G. Pozina, J.H. Yang, J. Appl. Phys. 108 (2010) 103513.
[40] L. Covington, J. Moore, Thin Solid Films 540 (2013) 106.
[41] B.E. Jun, Y.S. Kim, B.K. Moon, B.C. Choi, J.H. Jeong, H. Choi, J. Kim, S.S. Yi, J. Korean Phys. Soc. 53 (2008) 1655.
[42] S.A. Studenikin, Nickolay Golego, Michael Cocivera, J. Appl. Phys. 83 (1998) 2104.
[43] J. Singh, Electronic and Optoelectronic Properties of Semiconductors Structures, Cambridge University Press, Cambridge, 2003.
[44] P.D.C. King, T.D. Veal, C.F. McConville, Phys. Rev. B 77 (2008) 125305.
[45] M. Abramowitz, I.A. Stegun, Handbook of Mathematical Functions (New York, Dover, 1970).